Optogenetic Control of Programmable Genome Editing by Photoactivatable CRISPR/Cas9 Nanosystem in the Second Near-Infrared Window

Xiaohong Chen[1], Yuxuan Chen[1], Huhu Xin[1], Tao Wan[1], Yuan Ping[1]

[1]College of Pharmaceutical Sciences, Zhejiang University, Hangzhou 310058, China

These authors contributed equally: Xiaohong Chen, Yuxuan Chen.
Corresponding and requests for materials should be addressed to Y.P. (email: pingy@zju.edu.cn)

Abstract

We herein report the first optogenetically activatable CRISPR/Cas9 nanosystem for programmable genome editing in the second near-infrared (NIR-II) optical window. The nanosystem is composed of a cationic polymer-coated gold nanorod (APC) and Cas9 plasmid driven by a heat-inducible promoter. APC not only serves as a carrier for intracellular plasmid delivery, but also can harvest external NIR-II photonic energy and convert into local heat to induce the gene expression of Cas9 endonuclease. Due to high transfection activity, APC shows strong ability to induce significant level of disruption in different genome loci upon optogenetic activation. Moreover, the precise control of genome editing activity can be simply programmed by finely tuning exposure time and irradiation times in vitro and in vivo, and also enables editing at multiple time points, thus proving the sensitivity and reversibility of such an editing modality. The NIR-II optical feature of APC enables therapeutic genome editing at the deep tissue of the tumor-bearing mice, by which tumor growth could be effectively inhibited as a proof-of-concept therapeutic example. Importantly, this modality of optogenetic genome editing can significantly minimize the off-target effect of CRISPR/Cas9 in the most potential off-target sites. The optogenetically activatable CRISPR/Cas9 nanosystem we have developed offers a useful tool to expand the current applications of CRISPR/Cas9, and also defines a programmable genome editing strategy towards unprecedented precision and spatiotemporal specificity.

Introduction

The RNA-guided clustered, regularly interspaced, short palindromic repeats (CRISPR)-associated nuclease protein 9 (Cas9) is originally an adaptive immune defense system, by which many bacteria exploit to protect themselves from invading genetic elements[1]. It has been recently harnessed as an efficient tool for genome editing in both single cells and the whole organism for a wide range of biomedical applications in biology, genetics, and medicine, etc[2,3]. In principle, the CRISPR/Cas9 is composed a single-guide RNA (sgRNA) for the identification of DNA targets and a Cas9 endonuclease that can bind and process the recognized DNA targets[4]. CRISPR/Cas9-based genome editing technology offers a powerful and reliable strategy for the targeted modifications of the genome, enabling the precise perturbation of virtually any genomic sequence in living cells[2-6]. Due to its genome-wide specificity and multiplexing capability, Cas9 and its variants have shown great potentials in the generation of loss-of-function animals[7,8], the correction of genetic disorders[9,10], functional genome screening[11-15], and the treatment of infectious diseases[16,17]. Despite of these excitements, the lack of temporal and spatial precision during editing process has severely constrained the current CRISPR/Cas9 systems from complicated and diverse genome-editing scenarios. Furthermore, off-target activity has now become a major concern when the CRISPR/Cas9 system is exploited for therapeutic purposes.

To improve the spatiotemporal specificity of Cas9-mediated genomic manipulation, recent efforts have been dedicated to the development of inducible CRISRP/Cas9 architectures to enable the conditional control of Cas9 activity through either chemical[18-22] or optical[23-26] means. By precisely limiting the time of Cas9 function, the off-target activity is also expected to be controlled by minimizing the unwanted prolong Cas9 activity[19,26]. Chemical methods mainly refer to the regulation of endonuclease activity of

Cas9 through small-molecule-triggered Cas9 binding and self-splicing inteins[19-21]. Although a few examples have been illustrated for the temporal control of Cas9 activity[27-29], however, this strategy generally lacks spatial specificity and reversibility, making it difficult to be explored for in vivo studies. Furthermore, the commonly used small molecules for chemical activation, such as rapamycine[22] and doxycycline[19,21], may induce potential cytotoxicity towards both edited and non-edited cells[30]. As opposed to the chemical strategies, optical regulation of Cas9 function is more favorable in terms its non-invasiveness, spatiotemporal specificity and reversibility. In the past few years, several different photoactivatable systems have been adopted for the optical regulation of CRISPR/Cas9-based genome editing and transcriptional activation[31,32]. For example, photoactivatable Cas9 consisting of two split, deactivated Cas9 (dCas9) fragments and photoinducible dimerization domains (Magnets) was engineered to enable optogenetic control of CRISPR-Cas9 activity in human cells[26]. Upon blue light irradiation, the split Cas9 was fused to Magnet domains to recover its genome editing activity, which could be simply switched off by extinguishing the irradiation. More recently, optogenetic anti-CRISPR variants comprising a powerful Cas9 inhibitor (hybrids of AcrIIA4) and a LOV2 photosensor, were engineered for the photoregulation of CRISPR-Cas9 activity[33]. As the photoirradiation enabled the release of dCas9 from the optogenetic variant of AcrIIA4, the inhibited Cas9 activity could be rapidly recovered to enable genome and epigenome editing. Nevertheless, most optically controlled CRISPR/Cas9 systems reply on the photoactivation by blue light. This suggests these blue light-mediated activatable CRISPR/Cas9 systems are not only difficult for deep-tissue penetration through turbid human tissues, but also are potentially phototoxic in the realistic genome-editing applications. To address these issues, far-red light-mediated CRISPR-dCas9 device, which is built based on the bacterial photoactivatable cyclic diguanylate monophosphate (c-di-GMP) synthase BphS and the c-di-GMP-responsive hybrid transactivator, has been recently developed for the targeted epigenetic modulation both in vitro and in vivo[34]. Most recently, near-infrared upconversion-activated CRISPR-Cas9 nanoparticle system have been proposed for the optical control of therapeutic gene editing towards cancer treatment[35]. While above two studies revealed the infrared light is critical for the regulation of genome editing and epigenome editing in vivo, the precise CRISPR/Cas9 genome editing in a programmable, reversible manner has not been demonstrated yet, not to mention those for in vivo applications. In addition, off-target activity induced by light-controlled editing modalities still remains elusive to date.

We herein report the first photoactivatable CRISPR-Cas9 nanosystem for the optogenetic control of genome editing at the second near-infrared (NIR-II) optical window (1000 to 1700 nm). As shown in Scheme 1, this CRISPR/Cas9 nanosystem is typically composed of the cationic polymer-coated gold nanorod (AR) and the Cas9 plasmid driven by a heat-inducible promoter, HSP70 (HSP-Cas9). Whereas the cationic polymer is able to carry and deliver the plasmid into the targeted cells, the gold nanorod serves a photothermal transducer to transform the harvested external light into the intracellular local heat. As such, APC not only acts as the delivery carrier for the plasmid delivery, but also serve as an intracellular photothermal converter to trigger the transcription of Cas9 and sgRNA. By incorporating the expression vector with Cas9 gene cloned downstream of a heat-inducible HSP70 promoter, the elevated local temperature subsequently offers a cue to promote the gene expression of Cas9. Thus, Cas9 activity can be regulated by heat-induced gene expression and activated by photothermal signals. APC/plasmid is first internalized by the targeted cell through charge-mediated internalization, followed by the formation of endosomes. After the endosomal escape, whereas the plasmid released

from APC enters into nucleus, APC still retains in the cytoplasm. Once upon the light irradiation at 1064 nm, APC quickly generates localized heat in the intracellular microenvironment to induce the transformation of heat shock factor (HSF) from inactive monomers to active trimmers, which are capable of translocating into the nucleus. Then, the binding of intranuclear trimmers to heat shock element (HSE) of the HSP70 promoter results in the activation of transcription[36]. However, once the light irradiation is switched off, the decreased temperature releases the bound trimmer from HSE, triggering the re-transformation of trimmers back to monomers to inactivate the transcription process[37]. Thus, APC acts as an optogenetic switch to regulate Cas9 expression and activity with high spatiotemporal specificity. As NIR-II light shows a stronger tissue-penetration ability as compared with the first NIR (NIR-I) light (650-950 nm), the regulation of genome editing in vivo is also affordable by APC through the optogenetic control in the NIR-II optical window. As we found in our study, APC-mediated optogenetic activation and spatiotemporal control of gene expression are demonstrated to direct Cas9 activity in a precise and programmable manner, and significantly reduce off-target effects in the current study, thereby paving a safe way for in vivo therapeutic genome editing and the spatiotemporal control of CRISPR/Cas9 in vitro and in vivo.

Results

In our study, the classic cetyltrimethylammonium bromide (CTAB)-mediated synthesis approach was used for the preparation of gold nanorods[38,39], and uniform ARs with an aspect ratio of 7.1 (length = 106.4 ± 14.1 nm, width = 15.2 ± 3.3 nm) were obtained (Fig. 1a). Afterwards, biocompatible polystyrene sulfonate (PSS), which acted as an interconnecting layer, was then coated on the AR surface through the electrostatic force to form PSS-coated ARs. Subsequently, β-cyclodextrin-PEI (CP), a cationic polymer that has been well demonstrated for the efficient transfection of plasmids for both in vitro and in vivo[40-42], was assembled on the top of the PSS layer. The layer-by-layer assembly process to prepare APC was verified by zeta potential analysis (Fig. 1b), where the final product APC showed a positive surface charge. AR displayed a strong, brand absorption in the NIR-II region, with an absorption peak at ca. 1070 nm (Fig. 1c). Noticeably, the assembly of polyelectrolytes on AR merely affected the wavelength of maximum absorption. Such a NIR-II optical feature is crucial for in vivo investigations. Upon continuous laser irradiation at 1064 nm for 5 min, the temperature of APC solution quickly increased and achieved the plateau of 42 °C under a power density at 0.33 W/cm^2, as recorded by the infrared thermal camera (Fig. 1d). The maximum temperature generated by APC could be further adjusted to 65 °C at a power density of 1.00 W/cm^2. The repeated heating and cooling of 3 cycles resulted in similar temperature fluctuation (Supplementary Fig. 1), and laser irradiation merely changed the morphology of APC (Supplementary Fig. 2), thus demonstrating its superior photothermal stability. As the optimal temperature for the activation of the HSP70 promoter was approximately 42 °C[43], we also explored the irradiation mode that could stabilize the temperature at this degree. By discontinuous irradiation, the temperature could be finely tuned to a narrow range from 39.0-42.0 °C (Supplementary Fig. 3). Given the temperature elevation would start from body temperature for in vivo activation, we explored the fine temperature control starting from 37 °C by discontinuous irradiation, and found this irradiation approach could likewise control the temperature in an ideal range (39.0-42.0 °C) by slightly adjusting the discontinuous irradiation time (Supplementary Fig. 4). We thus adopted this discontinuous irradiation mode to control the temperature for the subsequent experiments for the activation of CRISPR/Cas9 systems in vitro and in vivo. In the

meantime, high-angle annular dark field scanning transmission electron microscopy (HAADF-STEM) and energy dispersive X-ray spectroscopy (EDS) mapping were performed to verify the layer-by-layer (LBL) structure of APC/HSP-Cas9 (Fig. 1e). The distribution of S, N or P element well overlapped with the Au element. The LBL structure of APC/HSP-Cas9 complexes was also determined by X-ray photoelectron spectroscopy (XPS). In the survey spectra of APC/HSP-Cas9 complexes (Fig. 1f), the peak of S2p belonged to the PSS coating, and the peak of N1s was corresponded to the nitrogen atoms in the CP and plasmid DNA. Cl2p and NaKLL was attributed to the salts in the buffer. In N1s and S2p spectrum of AuNR-CTAB and AuNR-PSS, the peaks of 402 eV belonged to the quaternary amine of CTAB (Supplementary Fig. 5a), and the appearance of S2p peak proved the coating of PSS in AuNR-CTAB (Supplementary Fig. 5b). After coating of CP, the peak A (401.9 eV) decreased, whereas peak B and peak C (400.2 eV, 398.4 eV) that were attributed to the CP clearly increased (Supplementary Fig. 5c)[44,45]. When APC was complexed with plasmid DNA, the elimination of peak A was due to the shielding effect after DNA complexation with APC (Supplementary Fig. 5d). To demonstrate whether APC was able to encapsulate the plasmid encoding Cas9 and luciferase, gel electrophoresis assay was first carried out. APC could completely inhibit plasmid DNA migration at APC/plasmid weight ratio of 0.15, proving its excellent capability to condense and carry plasmid DNA for gene transfection (Fig. 1g).

In the current, we constructed the Cas9-encoding plasmid driven by a HSP70 promoter. The plasmid consists of a Cas9 gene driven by HSP70 promoter (Supplementary Table 1), an EGFP reporter and a luciferase reporter downstream of Cas9, all of which are separated by self-cleaving peptides P2A, followed by a segment of independent sgRNA sequence driven by U6 promoter downstream of luciferase reporter. To mark Cas9 expression, the two reporters EGFP and luciferase, which is also driven by HSP70 promoter, can express with Cas9 simultaneously (Fig. 1h). Therefore, we first checked the GFP expression after the intracellular delivery of APC/HSP-Cas9 complexes. As shown in Fig. 1i, very weak fluorescence generated from green fluorescence protein (GFP) was observed in the 293T cells without laser treatment, implying the low background activity. In sharp contrast, strong green fluorescence was observed after the light irradiation on the cells. Flow cytometry analysis indicated that after APC-mediated transfection and photothermal activation, the percentage of GFP-positive cells reached more than 90% under the laser irradiation, which is much higher than that from the transfection supported by Lipofectamine 2000 (Lipo, commercially available transfection agent) or PEI (non-viral ‘gold standard’ transfection agent) at 42 °C (Fig. 1j and Supplementary Fig. 6). The high level of gene expression was further corroborated by luciferase reporter assay, where strong luciferase expression was detected when the transfection was mediated APC with laser irradiation (Supplementary Fig. 7). The incorporation of sgRNA cloned downstream in the plasmid merely affected the transfection activity of APC (Supplementary Fig. 8). In the meantime, Bio-TEM image indicated that APC was primarily located in the cytoplasm after the GFP expression (Fig. 1k). These results suggested that APC could not only mediate efficient transfection, but also trigger HSP70-regulated gene expression upon photothermal activation. In the meantime, we found that the level of luciferase expression could be modulated by laser intensity (Supplementary Fig. 9) and irradiation time (Supplementary Fig. 10), implying the transgene expression level is precisely tunable. In order to elucidate the role of specific internalization pathways, different inhibitors were added to the cell culture medium before the transfection in 293T cells (Supplementary Fig. 11-12). It was evident that the addition of methyl- β -cyclodextrin significantly reduced GFP expression,

suggesting the internalization of APC/pDNA complexes primarily follows the caveolae-dependent endocytosis. Additionally, the inhibition of transfection activity by bafilomycin A1 suggested the strong buffering capacity of APC, which is critical to facilitate the endosomal escape of the delivered plasmids. APC also showed high transfection activity towards different types of cell lines upon photothermal activation (Supplementary Fig. 13), which paves the way for the optogenetic control for CRISPR/Cas9 genome editing activity for an array of biomedical purposes.

Based on the above optimized results, we subsequently investigated whether optogenetic control of CRISPR/Cas9 activity could be manipulated through efficient transfection and photothermal conversion by APC (Fig. 2a). First, we tested whether APC was capable of disrupt enhanced green fluorescence protein (EGFP) gene in 293T cells that stably expressed EGFP (Fig. 2b). Upon the intracellular delivery of APC/HSP-Cas9 targeting EGFP, the intensity of GFP in 293T-EGFP cells decreased significantly with the laser irradiation, suggesting the strong ability of APC to mediate the disruption of GFP gene. Nevertheless, the treatment with APC/HSP-Cas9-sgEGFP without laser irradiation had negligible knockout effects. To further validate the genome editing efficiency, we studied the intracellular delivery of HSP-Cas9 plasmid targeting different genome loci in the 293T cell line. Indels (insertion and deletion) detected by T7 Endonuclease I (T7E1) digestion assays were carried out to evaluate the efficiency of genome editing at the targeted genome sites. After the transfection and the photothermal activation, the bands from the digestion products of T7E1 distinguishing indels in the double-stranded DNA, were clearly detected from the uncut bands at the genomic locus of adeno-associated virus integration site 1 (*AAVS1*). We noted that the editing efficiency is slightly dependent on the APC concentration, with the highest indel rate of 20.1% at the APC/plasmid weight ratio of 1:2. As expected, *AAVS1* genome editing by Lipo and PEI resulted in the indel rate of 8.9% and 3.3%, respectively, both of which were lower than that of APC-mediated genome editing (Fig. 2c). Sanger sequencing confirmed indels at the targeted loci, including base deletion, insertion and substitution around the protospacer adjacent motif (PAM) (Fig. 2d, Supplementary Fig. 14). In the meantime, we further investigated whether the level of GPF expression is synchronized with the Cas9-mediated genome disruption. As expected, the level of GFP expression was well correlated with the indel rate, suggesting the level of GFP expression could well reflect and estimate the indel rate (Fig. 2e). Similarly, by screening different sequences of sgRNA (Supplementary Table 2, 3), the optimized genome editing at rhomboid family member 1 (*RHBDF1*) locus mediated by APC showed an indel rate of 14.8%, which is more efficient than that of Lipo (6.5%, Fig. 2f) and confirmed by Sanger sequencing (Supplementary Fig. 14). Furthermore, we examined whether the optogenetic control could likewise activate the multiplex genome editing. To this end, we delivered two plasmids, both of which encoded a single but different sgRNA construct targeting *AAVS1* and *Plk1* (polo-like kinase 1), respectively. Both genome loci showed evident degree of editing, with the indel rates of 28.8% (*AAVS1*) and 37.0% (*Plk1*) (Fig. 2g, h). Since APC can well absorb NIR-II light that can afford deep-tissue penetration, we covered the cell culture plate with the breast chicken tissue of different thickness and investigated whether the irradiation could still activate the genome editing in the transfected cells in the presence of tissue (Fig. 2i). Though the increase of the tissue thickness impaired the genome editing activity, the indel (6.6%) could be still detectable in the presence of 12 mm of breast chicken tissue. This suggested that the increase in the tissue thickness slightly impaired the penetration ability of NIR-II light, thereby affecting the photothermal conversion efficiency as we have demonstrated (Supplementary Fig. 15). Furthermore,

the luciferase expression was temperature-dependent and became evident when the temperature reached 39 °C, reaching the highest at 42 °C (Supplementary Fig. 16). The above data suggest that the temperature window between 39 to 42 °C is optimal for optogenetic activation of Cas9 transcription. Interestingly, such optogenetic activation also works well for dCas9-mediated transcriptional activation of exogenous genes. For example, when three plasmids (HSP-dCas9-SPH, U6-sgRNA, and miniCMV-mCheery) were co-transfected in 293T cells, only very low basal fluorescence was observed before optogenetic activation, due to the weak ability of miniCMV to induce transcription. In sharp contrast, mCherry expression became very strong after the transcriptional activation of the heat-shock promoter, suggesting its potential towards heat-inducible transcriptional activation (Fig. 2j). In the meantime, we investigated whether such a heat-shock approach affected cell cycles and induced potential apoptosis (Supplementary Fig. 17). As expected, cells treated with APC/HSP-Cas9 complexes with or without laser irradiation showed similar cell-cycle pattern as those treated with PBS. In the meantime, cell transfected with APC/HSP-Cas9 complexes merely induce any apoptosis, suggesting the biocompability of APC and the safety of heat-shock optogenetic modality. Collectively, these results strongly suggested that the control of genome editing activity could be manipulated through optogenetic activation of CRISPR/Cas9.

While successfully establishing above strong evidence of optogenetic genome editing, we are curious about whether such a modality could precisely control the degree of editing. We first monitored the continuous bioluminescence (BL) intensity to reflect the amount of Cas9 expression upon the optogenetic activation, and incremental percentage of BL was studied as a function of time. As reflected by Fig. 3a, after the transfection for 24 h, the BL intensity increased quickly once the laser was switched on, and reached the plateau after the laser irradiation for only 5 min, suggesting a fast and enhanced gene expression by optogenetic activation. However, the level of luciferase expression dropped slightly after this time point, and significantly decreased to the basal level upon the removal of irradiation. However, when the laser switched on again 24 h after the first irradiation, BL intensity rapidly increased again, and decreased upon the removal of irradiation. The above information suggested photothermal control of gene expression by APC is reversible, and APC may serve as an optogenetic switch to regulate Cas9 expression and activity. These findings further stimulated us to explore how the level of genome editing could be precisely controlled through this optogenetic switch we have developed. By controlling the time length of irradiation from 5 to 30 min, we found the indel range could be precisely tuned from 3.4% to 31.4% (Fig. 3b, c), which was also reflected by GFP expression with different irradiation time (Supplementary Fig. 18). Furthermore, the temporal control of genome editing activity could also be simply realized by adjusting the number of irradiation times (Fig. 3d). When the irradiation was conducted for only one time (30 min), the resulted indel rate was 11.5%; however, the indel rate could be improved simply by increasing the number of irradiation times to reach the expected ones (Fig. 3e, f). It is worthy to mention that such a stepwise, optogenetic activation modality is also highly stable. By analyzing the indel rate at different time points, we found the degree of editing was generally stable over a period of 36 h, irrespective of the irradiation times (Fig. 3g-j).

To validate the potential of such an optogenetic control modality in vivo, A549 cells transfected with APC/HSP-Cas9 complexes were subcutaneously transplanted into the back of the BALB/c mice ex vivo. The treated mice were monitored by a thermal camera to ensure that the temperature in the irradiation position remain stable. Following the

laser irradiation on the subcutaneous transfected cells, BL intensity gradually became strong along the increased irradiation time, suggesting the successful optogenetic activation of gene expression in a heat-inducible, finely tuned manner (Fig. 4a). We next harvested these transplanted cells and checked whether the optogenetic activation works for in vivo genome editing. As shown from T7E1 assay results (Fig. 4b, c), indel rate ranging from 4.7% to 20.1% could also be well manipulated by tuning the irradiation time, implying the controllable activation of Cas9 expression and programmable regulation of genome editing activity in vivo. Moreover, we explored whether direct in vivo transfection and optogenetic activation is possible. To this end, APC/HSP-Cas9 complexes were first delivered into the hind limb of BALB/c mice via intramuscular injection (IM), and the optogenetic activation was conducted after 8 h (Fig. 4d). Strikingly, strong in vivo bioluminescence was clearly detected in the hind limb 40 h after the optogenetic activation. Based on these findings, we further harvested and lysed the tissue from the muscle of the hind limb to evaluate the indel mutation of the edited cells. The indel rate reached 18.1% with the laser irradiation, however, without laser irradiation, the indel was hardly detectable after the in vivo transfection of APC/HSP-Cas9 complexes (Fig. 4e, f). This further motivated us to explore whether optogenetic genome editing could be manipulated in the deep tissue of local lesions, since NIR-II light have deeper penetration capability over the NIR-I light. For this purpose, BALB/c nude mice bearing A549 xenograft tumor were first injected with APC/HSP-Cas9 complexes through peritumoral injection, and the irradiation was then carried out in the presence of a piece of breast chicken tissue (5 mm of thickness) covering the tumor position to simulate the deep-tissue condition (Fig. 4g). Excitingly, strong BL intensity was clearly observed over the tumor tissue (Fig. 4g). The tumor temperature was detected as 40.0 to 41.4 °C, suggesting that moderate hyperthemia could well activate the gene expression (Fig. 4g). In the meantime, significant level of genome editing was detected from both surface and deep layer of the tumor tissues, with an indel rate of 16.0% and 14.9%, respectively (Fig. 4h, i). These results strongly implied that such an optogenetic control may be suitable for regulating genome editing activity in deep-tissue environment. Given that the elevated temperature improved the Cas9 activity[46], such a heat-shock approach may also improve the editing capacity of the optogenetically activatable nanosystem. Furthermore, the spatiotemporal specificity could be well manipulated as well though the opogenetic regulation. The systemic administration of APC/HSP-Cas9 of BALB/c mice by tail-vein injection resulted in strong luciferase expression in the liver that is exposed to irradiation (Fig. 4j, Supplementary Fig. 19). In agreement with the results from transcriptional activation of exogenous gene in vitro, the transcriptional activation of mCherry expression was also verified in vivo, when APC/plasmids complexes were co-delivered into the hind limb either through ex vivo transfection or direct in vivo tissue transfection, followed by optogenetic activation (Fig. 4k, l, Supplementary Fig. 20). Importantly, we demonstrated that the optogenetic activation though different administration approaches, including ex vivo transfection, direct in vivo intramuscular administration, and systemic administration, merely induced toxicity in the major organs (heart, liver, spleen, lung, and kidney) after the irradiation (Supplementary Figs. 21-23). The above results demonstrated that the spatiotemporal and programmable genome editing could also be safely achievable in vivo as well.

As a proof-of-concept example for therapeutic genome editing, we further investigated whether the optogenetic activation of CRISRP/Cas9 nanosystem is possible for cancer therapy. To this end, we first delivered Cas9 plasmid with sgRNA targeting *Plk1*, a master regulator of mitosis[47], and activated the expression after the transfection in A549

cells. Indel analysis indicated that significant mutation was detected in the targeted genome locus, with an indel rate up to 41.5% when the optimized sgRNA targeting *Plk1* was used. (Fig. 5a). The editing-induced indel was also confirmed by Sanger sequencing results, where significant deletion and insertion was detected at the targeted loci around the PAM (Fig. 5b, Supplementary Fig. 14). Western blot analysis indicated that the level of *Plk1* expression remarkably reduced after the transfection and activation process (Fig. 5c). These results in vitro well establish the fact that optogenetically regulated genome editing enables the efficient knockout of target *Plk1* gene. We next investigated whether the tumor growth could be effectively inhibited on BALB/c nude mice bearing A549 xenograft tumor by this therapeutic modality (Fig. 5d). After the peritumoral injection of APC/HSP-Cas9 complexes, 48 h, we noticed that the BL was still visible, but became weak after irradiation activation (Fig. 5e). In the meantime, T7E1 assay results suggested the significant genome disruption in *Plk1* site in the tumor tissue (Fig. 5f, g). Thereby, the reduced expression was probably attributed to the presence of large amounts of apoptotic cells induced by *Plk1* disruption, leading to the poor ability to express luciferase. In fact, the above speculation is verified by the in vivo tumor inhibition assay, where the tumor-bear mice injected with APC/HSP-Cas9 targeting *Plk1* exhibited significant tumor regression after the irradiation treatment. The tumor size also became much smaller in comparison with the initial size before treatment. In sharp contrast, the mice treated with the same formulation, but without laser treatment exhibited rapid tumor progression, reaching a final tumor volume of 1270 mm^3 at the 21 day (Fig. 5h, i). As an indicator of systemic toxicity, we monitored the body weight through therapy session, and noticed that a slight increase in body weight was observed at the end of the treatment (Fig. 5j). In the meantime, the toxicity to major organs was investigated by H&E staining (Supplementary Fig. 24), and blood biochemistry was also evaluated to reflect liver and kidney index (Supplementary Fig. 25). As compared with saline control group (without laser treatment), the tumor slice showed fewest tumor cells combined significant degree of necrosis. Whereas H&E staining suggested that such a therapeutic modality was generally safe and biocompatible in the major organs, the function index of blood biochemistry further validated that such an optogenetic treatment merely caused any damage to the liver and the kidney. These results collectively demonstrated such an optogenetic activatable CRISPR/Cas9 nanosystem provides a new strategy for programmable genome editing with unrivaled spatiotemporal specificity in vivo.

To analyze the off-target effects generated by this editing modality, we used an off-target searching tool, Cas-OFFinder to estimate the potential off-target sites and carried out T7E1 assay to evaluate whether gene mutations could be detected in the estimated off-target sites. Sanger sequencing analysis proved that the sequence that was suspected to off-target disruption displayed the same intact sequence as the wild-type one without any treatments (Supplementary Fig. 26), suggesting the high on-target activity with minimum off-target effect. These results collectively demonstrated that optogenetically activatable CRISRP/Cas9 nanosystem may minimize off-target effects through optogenetic control of Cas9 expression to reduce prolonged Cas9 activity.

Discussion

Remote activation with non-invasive NIR light has been extensively exploited in wide range of biomedical applications, such as microRNA detection[48], brain stimulation[49], modulation of gene expression[43], and immunomodulation[50], largely owing to the low photocytotoxicty and deep-tissue penetration capability of NIR light. To date, reports on

the optical control of CRISPR/Cas9 function with infrared light are very rare, not to mention those in NIR-II window. The recent advances in NIR-II-absorbing photothermal nanomaterials provide new possibilities to convert photonic energy into heat in the localized position at the NIR-II window. In comparison with the NIR-I light, NIR-II light has been validated to afford deeper tissue penetration, a key challenge preventing many optogenetic control strategies from in vivo investigations. Although a few types of organic[51-53] and inorganic nanomaterials[39,53] that absorb NIR-II light have been developed, AR was selected as a building block for APC largely due to its high photothermal conversion rate and photothermal stability[54]. Furthermore, the AR not only converts the external photonic energy into the intracellular local heat, but also serves as a template where the cationic polymers are assembled for the subsequent encapsulation of large plasmids. As an unconventional finding, the assembly of PC over AR surprisingly resulted in far more efficient condensation of Cas9 plasmid in comparison with PC alone[42], probably owing to the higher aspect ratio of gold nanostructure more favorable for entangling the plasmid. This feature of AR may also facilitate APC to enter nucleus by passive fusion, as high-aspect-ratio nanoparticles, such as nanorods and nanoworms, were previously demonstrated to be superior to the spherical ones with identical surface chemistries in terms of nuclear entry[55]. It is also noteworthy that the incorporation of Cas9 plasmid and photothermal transducer into the same carrier ensures the delivery of two payloads into the same cell population, thereby maximizing the sensitivity and efficiency of optogenetic activation of the Cas9 transcription.

Heat-induced transcription of genes encoding a major heat-shock protein (HSP70) is a cytoprotective mechanism by which a wide variety of cells exploit to protect themselves from heat shock and other deleterious stresses[56]. HSP70 promoters are regulated by cytosolic HSF, which becomes active in response to moderate hyperthermia (39 °C to 42 °C) to induce the expression of downstream heat-shock proteins that are critical for cellular defense[57]. The heat-responsive HSP70 promoters have been previously explored for the spatial and temporal control of gene expression through photothermal effects[58-60]. In the current study, we constructed the Cas9-encoding plasmid driven by a HSP70 promoter, which indeed serves as a photothermal switch to regulate the Cas9 transcription by sensing the surrounding temperature. Such a design strategy for heat-inducible transcription is also affordable for dCas9-mediated transcription activation, and is expected to extend for a wide range of CRISPR/Cas-based potential applications. As the temperature could be finely tuned by controlling the irradiation time length and is closely correlated to Cas9 expression and activity, we are therefore capable of programming the degree of editing simply by adjusting exposure time and irradiation times. Hence, this editing modality may be applicable to the context where CRISPR/Cas9 activity is required to fulfill editing missions at multiple time points. For example, the optogenetically activatable CRISPR/Cas9 nanosystem may serve as an ideal platform for inducible editing at multiple time points that is required for CRISPR/Cas9 barcode editing to trace lineage information of different cells during development and diseases[61]. For many other applications, CRISPR/Cas9 activity should be inhibited following the on-target editing, and prolonged activity may otherwise cause undesired side effects. For instance, restriction of Cas9 activity to a narrow temporal window is critical in germline editing, as the persistent Cas9 activity following the initial rounds of mitosis contributes to mosaicism[62,63]. Collectively, our system also provides a robust method to diminish Cas9 activity after certain editing events simply by switching off the light.

Spatiotemporal specificity of CRISPR/Cas9 is essential for many potential therapeutic purposes in that Cas9 activity in ancillary tissues may give rise to safety risks. As a proof-of-concept study, we demonstrated that the spatiotemporal control of CRISPR/Cas9 activity can well be manipulated through optogenetic activation. Thanks to the NIR-II-absorbing feature of APC, the spatial optogenetic control is validated to be realizable in deep tissue, which opens an avenue for broader in vivo investigations. In addition, the current findings also suggest that precise control of Cas9 activity by light is important to diminish off-target effect and other genotoxicities[64]. Our future efforts will be dedicated to the intensive investigations of off-target effects at the whole-genome level, in order to understand the safe use of this genome-editing modality.

Materials and Methods

Materials

Sodium borohydride ($NaBH_4$), silver nitrate ($AgNO_3$), hydroquinone (HQ), Dulbecco's modified Eagle's medium (DMEM), polyethyleneimine (PEI, MW: 25k Da) and D-luciferin-K+ salt bioluminescent substrate was purchased from Sigma-Aldrich (USA). Tetrachloroauric(III) acid trihydrate ($HAuCl_4 \cdot 3H_2O$), cetyltrimethylammonium bromide (CTAB), poly(sodium 4-styrenesulfonate) (PSS, MW ~70,000 g/mol) were purchased from Aladdin (China). The cell counting kit-8 (CCK-8) was obtained from DOJINDO (Japan). Propidium iodide (PI), Calcein acetoxymethyl ester (Calcein AM), penicillin−streptomycin, phosphate-buffered saline (PBS), fetal bovine serum (FBS) and Lipofectamine 2000 (Lipo) were purchased from Thermo Fisher Scientific (USA). Cell cycle and apoptosis analysis kit were purchased from Beyotime (China). T7 endonuclease I (T7E1) enzyme was purchased from GenScript (USA). Ultrapure water was used in all experiments. Antibodies used in this project included the following: *Plk1* antibody (#4535) and anti-GAPDH (#2118) were obtained from Cell Signalling Technology (USA). 1064 nm low power NIR Laser was purchased from Fingco (China).

Synthesis of Gold Nanorods (ARs)

ARs were synthesized using a seed-mediated growth method as previously described[38,39] with minor modification. Briefly, the seed solution was first synthesized by adding freshly prepared 600 μL $NaBH_4$ (10 mM) into 5 mL mixture of $HAuCl_4 \cdot 3H_2O$ (0.5 mM) and CTAB (0.1 M), followed by being kept at 30 °C for 30 min to exhaust excess $NaBH_4$. The growth solution containing a mixture of 5 mL $HAuCl_4 \cdot 3H_2O$ and 5 mL CTAB (0.2 M), 120 μL $AgNO_3$ (0.1 M) and 600 μL HQ (0.1 M) were added in sequence. When the solution color turned from yellow to colorless, 320 μL seed solution was added to the growth solution. AuNRs with the desired longitudinal surface plasmon resonance (LSPR) peak were obtained after keeping the reaction mixture undisturbed in dark at 30 °C for 12 h. Finally, the ARs were collected by centrifugation at 7000 rcf for 10 min at 30 °C. The supernatant was removed and precipitate was resuspended in 2 mL 30 °C ultrapure water.

Synthesis of APC

For the synthesis of AR-PSS, ARs were first coated with PSS by the previous reported method[65]. In brief, 1 mL of AR solution (0.2 mg/mL Au) were added to 10 mL of PSS (2 mg/mL) dissolved in NaCl (1 mM) solution and stirred for 1 h at 30 °C. A centrifugation cycle of 7000 rcf for 10 min, and the residue was re-suspended to obtain 2 mL PSS-coated AR (AR-PSS) solution. β-CD-PEI which was synthesized by our reported method[40-42] was further coated onto AR-PSS using a similar method. 1 mL of AuNR-PSS

were added to 10 mL of β-CD-PEI (2 mg/mL) dispersed in NaCl (1 mM) solution and stirred for 1 h at 30 °C to obtain AR-PSS-β-CD-PEI (APC).

Heat-inducible Cas9/dCas9 plasmids construction

To construct HSP70-Cas9-GFP-luciferase-U6-sgRNA plasmid, HSP70 promoter core sequence[66] was amplified from genomic DNA of 293T cells by PCR and inserted into pCS2-CMV-Cas9-P2A-GFP-P2A-luciferase-pA (Addgene #48138) by replacing CMV promoter through Hind III restriction site. U6-sgRNA fragment was also added to the plasmid by SalI. CMV-Cas9-GFP-luciferase plasmid was constructed by replaced HSP70 promoter with CMV promoter. Other plasmids (HSP-Cas9-U6-gRNA and HSP-Cas9-GFP-U6-gRNA) were constructed similarly using the same molecular cloning methods.

The plasmids of CRISPR-dCas9-based transcriptional activation system were constructed based on SPH system (an improved dCas9 activation system) according to the reported literature[67]. In brief, for HSP-dCas9 plasmid, dCas9-10×GCN4-P2A-SPH-T2A-GFP fragment was amplified from AP111 (Addgene #107307) by PCR, and inserted into the HSP70 promoter backbone plasmid. For exogenous mCherry activation, a weak promoter miniCMV was ligated to mCherry fragment, and one dCas9 target sequence (5'-GTCCCCTCCACCCCACAGTG-3') was added upstream of miniCMV-mCherry plasmid. U6-sgRNA plasmid also contained the same target sequence. For endogenous gene activation, only U6-sgRNA targeted 5'UTR of the candidate gene was co-transfected with HSP-dCas9 plasmid. The control plasmid CMV-dCas9 was constructed based on HSP-dCas9 plasmid by replacing its promoter.

Targets design and sgRNA plasmids construction

All the targets of candidate genes were designed by online tool platform of Feng Zhang's lab (http://crispr.mit.edu/) and (http://chopchop.cbu.uib.no/). Primers and oligos used in the synthesis of all sgRNA plasmids used in this work are listed in Supplementary Table 2. The annealed oligos were cloned into HSP-Cas9/dCas9 or CMV-Cas9/dCas9 plasmids through BbsI restriction site. The annealing and cloning protocol was followed to Zhang Lab's website (www.genomeengineering.org).

Cell culture and transfection

All mammalian cells (293T, A549, SW480, HeLa, MDA-MB-231, HepG2) were cultured in Dulbecco's Modified Eagle Medium with high glucose, supplemented with 10% fetal bovine serum and 1× penicillin-streptomycin, and maintained at 37 °C with 5% CO_2. Cells were passaged to maintain the confluency below 70%. Cell transfections were performed using APC or Lipo with 250 ng of Cas9/dCas9 plasmid and 250 ng of sgRNA plasmid per well for 48-well plate.

Gel retardation assays

The ability of APC to complex HSP-Cas9 plasmid DNA was examined through gel electrophoresis. All the sample stock solutions were prepared at a concentration of 1 mg/mL in distilled water and pH was adjusted to 7.4. Solutions were filtered (0.22 μm) and stored at 4 °C. HSP-Cas9 plasmid (0.2 μg in 2μL of TAE buffer) was mixed with an equal volume of APC solution at the weight ratios between 0 and 10. Each mixture was vortexed and incubated for approximately 30 min at room temperature and then analyzed on 2% agarose gel. Gel electrophoresis was carried out in TAE running buffer (40 mM Tris-acetate, 1 mM EDTA) at 120 V for 40 min in a JUNYI Electrophoresis Equipment (JY300, Beijing Junyi-Dongfang, China). DNA bands were visualized and imaged by a Gel Documentation System (c150, Azure Biosystems, USA).

In vitro optogenetic activation assay

Transfection studies were performed in human 293T (human embryonic kidney cell line) and A549 (human lung adenocarcinoma cell line) cells. In brief, 48-well plates were seeded with cells at a density of 1.0 × 10^5/well 24 h before transfection in 500 mL DMEM medium. After 24 h of incubation, the vector/DNA complexes at optimized weight ratios were prepared by adding the PEI (25 KDa), Lipo or APC into 800 ng of DNA aqueous solutions with volume of 50 μL dropwise, vibrated for a few seconds, and stand for 30 min at room temperature before transfection. The complexes were added into cells and transfected in the serum-free culture medium for 6 h respectively. Then, the medium was replaced with 500 μL of fresh medium supplemented with 10% FBS. After the incubation for another 8 h, the samples were irradiated with 1064 nm laser light (0.33 W/cm^2) for a total time of 30 min (or other predefined time length) in a discontinuous mode at 37 °C, which was controlled by the thermal camera (FLIR) to maintain a temperature fluctuation between 39 °C to 42 °C. The cells were further incubated under the same conditions to reach a total transfection time of 48 h. Cells were harvested after washing with PBS twice for T7E1 assay (details were described in the 'T7E1' assay session), or the measurement of luciferase activities (Single-Luciferase Assay System Kit, Thermo Fisher Scientific).

Cellular uptake, cell cycle and cell apoptosis assay

293T and A549 cells were seeded in a 12-well plate with the density of 1.5 × 10^5 cells per well, the medium was replaced with serum-free medium after 24 h for transfection. APC/plasmid complexes (20 μL, 0.8 μg plasmid) at different APC concentrations were added into each well. After 6 h incubation, medium was replaced with fresh serum medium again. After another 2 h, cells were irradiated with 1064 nm laser light (0.33 W/cm^2) for 30 min at 37 °C, which was monitored by the thermal camera to ensure the temperature was always below 42 °C. After being incubated for another 40 h, the cells were washed with PBS thrice. The measurement was conducted by a flow cytometer (DxFLEX, Beckman Coulter, USA), using PEI 25 KDa and Lipo as the control. The mean fluorescence intensity was determined by counting 1.0× 10^4 single cells. To determine the effect of APC complex or optogenetic activation of Cas9 on cell cycles, 293T and A549 cells were cultured in a 6-well plate with a density of 2.5 × 10^5 cells per well, and then APC complex was added with or without the laser irradiation for 30 min to maintain the temperature fluctuation between 39-42 °C. The cells were harvested and fixed in pre-cold 70% ethanol for overnight at 4 °C. Then, 0.1% RNase (Sigma Aldrich) was added, followed by stained cells with propidium iodide (PI) solution (1 μg/μL) at room temperature for 30 min. Approximately 1.0× 10^4 cells/sample were analyzed by flow cytometry (DxFLEX) with an excitation wavelength at 488 nm and an emission wavelength at 617 nm. Cell apoptosis assay was performed in 293T and A549 cells by Annexin V-FITC/PI Apoptosis Kit (KeyGEN BioTECH, China).

Optogenetic activation of genome editing

293T cells were seeded at a density of 5.0 × 10^4 cells/well in 48-well plate, and were transfected with APC/HSP-Cas9 (at the weight ratio of 1:2) after 24 h. Lipo was used as a control. The total amount of DNA was 500 ng per well. After the transfection for 8 h, the fresh medium was changed, then the cells were exposed to discontinuous irradiation for 30 min with laser light of 1064 nm (0.33W/cm^2) at 37 °C. The thermal camera was used to monitor to maintain the temperature fluctuation between 39-42 °C. After another 40 h of incubation, genomic DNA was isolated using Trelief Animal Genomic DNA Kit (Cat.

No.: TSP201-50, TSINGKE Biological Technology, China). sgRNA targeting *AAVS1*, *Plk1* and *RHBDF1* were also tested.

Optogenetic regulation of transcriptional activation

For dCas9-induced transcriptional activation assay, APC (0.45 μg) was complexed with three plasmids containing a mixture of HSP-dCas9-SPH (0.30 μg), U6-sgRNA (0.30 μg) and miniCMV-mCherry (0.30 μg). 48 h later, cell nuclear was stained with Hoechst 33342 and incubated for 15 min. The optogenetic activation of mCherry was visualized by a confocal laser scanning microscope (LSM-510, CLSM, Carl Zeiss, Germany).

T7E1 assay

The disruption in the targeted genome loci in cells were evaluated by T7 Endonuclease I (T7E1) assay. After the transfection, the cells were harvested to extract genomic DNA using Trelief Animal Genomic DNA Kit (TSINGKE Biological Technology, China). The genomic region flanking the Cas9 target site for each gene was amplified by PCR (primers were listed in the supplementary Table 3), and products were purified using TIANquick Midi Quantification Kit (TIANGEN BIOTECH,China). A total of 200 ng PCR products were used to perform T7E1 assay following the manufacturer's protocol. After the treatment with T7E1, products were analyzed by agarose gel electrophoresis (2% gel) and imaged with a gel documentation system (c150, Azure Biosystems, USA). Quantification of the fragmented PCR products was analyzed, and indel percentages were determined based on relative band intensities. The undigested band and digested band of gray level was calculated by ImageJ. Indel percentage analysis was calculated with the following formula: $[1-(1-\text{fraction cleaved})^{1/2}] \times 100\%$, where the fraction cleaved refers to the band intensity of each digested band relative to the band intensity of both digested bands and undigested band. For the analysis of genome disruption in the edited tissue, the transfected tissues were first homogenized, and were further analyzed according to the above protocols.

Off-target analysis

The most potential off-target sites that are corresponding to the on-target genome locus (*AAVS1*, *Plk1* and *RHBDF1*) were identified with an online tool, Cas-OFFinder (http://www.rgenome.net/cas-offinder/). All the off-target sites and primers for PCR amplification were listed in Supplementary Table 4 and Supplementary Table 5. Off-target analysis procedure was similar to on-target examination through T7E1 assay. The sequence of analyzed off-target sites were also evaluated by Sanger sequencing after the APC-mediated optogenetic activation.

In vivo optogenetic regulation of genome editing

Female BALB/c nude mice (6-8 weeks old) were fed in the Laboratory in Animals Centre, Zhejiang University, and were supplied with sterilized air, water, and food. All animal treatments or procedures were approved by the Laboratory Animal Welfare and Ethics Committee of Zhejiang University. For ex vivo transfection, A549 cells were transfected with APC/HSP-Cas9 complex with 10 μg of plasmid (APC/plasmid = 1:2, weight ratio). After incubation of 24 h, the transfected cells were trypsinized, suspended in PBS, and injected into two sides of dorsal part of mice with equal volume of cells (200 μL with 2.5×10^6 cells). After another 6 h, the right injection site was irradiated with 1064 nm laser light (0.33 W/cm^2) with different irradiation time from 5 min to 30 min. The irradiated area was monitored by the thermal camera to maintain a temperature fluctuation between 39 to 42 °C. At 48 h, D-luciferin (150 mg/kg, 200 μL) in PBS buffer was injected intraperitoneally,

and the animals were anesthetized with isoflurane before the luciferase intensity was evaluated by in vivo imaging system (IVIS® Spectrum, PerkinElmer) 15 min later. For the intramuscular injection, APC/HSP-Cas9 complexes in 100 μL PBS (20 μg plasmid, 10 μg APC) were injected into both hind limbs by intramuscular injection. After 8 h, the right injection site was under discontinuous laser irradiation for 30 min with 1064 nm laser light (0.33W/cm^2) at room temperature, and luciferase expression was examined by in vivo imaging system (IVIS® Spectrum, PerkinElmer). For optogenetic activation in liver, APC/HSP-Cas9 complexes with 10 μg of plasmid (APC/plasmid = 1:2, w/w) were injected through the tail vein. At 8 h, the liver site was irradiated with 1064 nm laser light (0.33 W/cm^2) about 30 min. 48 h later, D-luciferin (150 mg/kg, 200 μL) in PBS buffer was injected intraperitoneally, and the luciferase intensity was evaluated by in vivo imaging system. For dCas9-mediated transcriptional activation, A549 cells were transfected with APC/plasmids (APC/plasmid = 1:2, w/w) containing a mixture of HSP-dCas9-SPH (3.33 μg), U6-sgRNA (3.33 μg) and miniCMV-mCherry (3.33 μg). After incubation of 24 h, the transfected cells was trypsinized, suspended in PBS, and injected into two sides of dorsal part of mice with equal volume of cells (200 μL, 2.5× 10^6 cells). The irradiation and in vivo imaging procedure were described above. For transcriptional activation via intramuscular injection, APC/HSP-dCas9-SPH complexes in 100 μL PBS (HSP-dCas9-SPH (6.33 μg), U6-sgRNA (6.33 μg) and miniCMV-mCherry (6.33 μg) plasmid, 10 μg APC) were injected into both hind limbs by intramuscular injection. The irradiation and in vivo imaging procedure were similar as above.

In vivo optogenetic genome editing for inhibition of tumor growth

The xenografted tumors were inoculated by subcutaneous injections of 2 × 10^6 A549 cells (suspended in 0.2 ml of PBS) on the back of the nude mice. When the tumor size reached about 80 mm^3, APC/HSP-Cas9 complex containing 10 μg of PCS2-HSP-Cas9-luciferase-U6-sg*Plk1* and 25 μL APC complex (5 μM) was injected through the peritumor injection. The injected mice were randomly assigned to five groups with five mice in each group. After the injection, the nude mice were discontinuously irradiated for 30 min with 1064 nm laser light (0.33 W/cm^2) at room temperature, and the thermal camera was used to control the temperature fluctuations from 39 to 42 °C. 48 h later, the mice were anesthetized with isoflurane before the luciferase intensity was evaluated by in vivo imaging system (IVIS® Spectrum, PerkinElmer). Injections were conducted twice a week and the treatment continued for almost three weeks. At each time point, vernier calipers were applied to measure the size of solid tumors. Tumor volume was calculated by the following formula: Tumor volume = [length of tumor × (width of tumor)^2]/2. On day 22, the treated mice were sacrificed and tumor weight was recorded.

Statistical analysis

Cell viability, tumor volume and tumor weight were calculated by expressing the mean ± standard deviation (S.D.). The statistical significance was analyzed using Students' t-test. The p-value less than 0.05 was considered significant (*p < 0.05, **p < 0.01, ***p < 0.001, ****p < 0.0001). All data and Figures in this paper were analyzed and plotted by Graphpad prism 8.0.

References

1. Jinek, M. et al. A programmable dual-RNA-guided DNA endonuclease in adaptive bacterial immunity. *Science* **337**, 816–821 (2012).

2. Cox,D.B., Platt, R. J. & Zhang, F. Therapeutic genome editing: prospects and challenges. *Nat. Med.* **21**, 121–131 (2015).
3. Wan, T. et al. Material solutions for delivery of CRISPR/Cas-based genome editing tools: current status and future outlook. *Mater. Today* 2018.12.003.
4. Nishimasu, H. et al. Crystal structure of Cas9 in complex with guide RNA and target DNA. *Cell* **156,** 935–949 (2014).
5. Wang, H. X. et al. CRISPR/Cas9-Based genome editing for disease modeling and therapy: challenges and opportunities for nonviral delivery. *Chem. Rev.* **117**, 9874–9906 (2017).
6. Mout, R., Ray, M., Lee, Y. W., Scaletti, F. & Rotello, V. M. In vivo delivery of CRISPR/Cas9 for therapeutic gene editing: progress and challenges. *Bioconjug. Chem.* **28**, 880–884 (2017).
7. Yang, L. et al. Genome-wide inactivation of porcine endogenous retroviruses (PERVs). *Science* **350**, 1101–1104 (2015).
8. Jin, L. & Li, J. Generation of genetically modified mice using CRISPR/Cas9 and haploid embryonic stem cell systems. Zool. *Res*. **37**, 205–213 (2016).
9. Min, Y. L., Bassel-Duby, R. & Olson, E. N. CRISPR correction of duchenne muscular dystrophy. *Annu. Rev. Med.* **70**, 239–255 (2019).
10. Yang, Y. et al. A dual AAV system enables the Cas9-mediated correction of a metabolic liver disease in newborn mice. *Nat. Nanotech*. **34**, 334–338 (2016).
11. Shalem, O., Sanjana, V. M. & Zhang, F. High-throughput functional genomics using CRISPR–Cas9. *Nat. Rev. Genet.* **16**, 299–311 (2015).
12. Joung, J. et al. Genome-scale CRISPR-Cas9 knockout and transcriptional activation screening. *Nat. Protoc*. **12**, 828–863 (2017).
13. Ting, P. Y. et al. Guide swap enables genome-scale pooled CRISPR–Cas9 screening in human primary cells. *Nat. Methods* **15**, 941–946 (2018).
14. Manguso, R. T. et al. In vivo CRISPR screening identifies Ptpn2 as a cancer immunotherapy target. *Nature* **547**, 413–418 (2017).
15. Yamauchi, T. et al. Genome-wide CRISPR-Cas9 screen identifies leukemia-specific dependence on a pre-mRNA metabolic pathway regulated by DCPS. *Cancer Cell* **33**, 386–400 (2018).
16. Liao, H. et al. Use of the CRISPR/Cas9 system as an intracellular defense against HIV-1 infection in human cells. *Nat. Commun*. **6**, 6413 (2015).
17. Scoppe, J. A. & Lebbink, R. J. Antiviral goes viral: harnessing CRISPR/Cas9 to combat viruses in humans. *Trends Microbiol*. **25**, 833–850 (2017).
18. Liu, K. I. et al. A chemical-inducible CRISPR–Cas9 system for rapid control of genome editing. *Nat. Chem. Biol*. **12**, 980–987 (2016).
19. Aubrey, B. J. et al. An inducible lentiviral guide RNA platform enables the identification of tumor-essential genes and tumor-promoting mutations in vivo. *Cell Rep*. **10**, 1422–1432 (2015).
20. Cha, P. H. et al. Small-molecule binding of the axin RGS domain promotes β-catenin and Ras degradation. *Nat. Chem. Biol*. **12**, 593–600 (2016).
21. Dow, L. E. et al. Inducible in vivo genome editing with CRISPR-Cas9. *Nat. Biotechnol.* **33**, 390–394 (2015).
22. Nguyen, D. P. et al. Ligand-binding domains of nuclear receptors facilitate tight control of split CRISPR activity. *Nat. Commun*. **7**, 12009. (2016).
23. Zhou, X. X. et al. A single-chain photoswitchable CRISPR-Cas9 architecture for light-inducible gene editing and transcription. *ACS Chem. Biol*. **13**, 443–448 (2018).
24. Hemphill, J., Borchardt, E. K., Brown, K., Asokan, A. & Deiters, A. Optical control of CRISPR/Cas9 gene editing. *J. Am. Chem. Soc*. **137**, 5642–5645 (2015).

25. Nihongaki, Y., Yamamoto, S., Kawano, F., Suzuki, H. & Sato, M. CRISPR/Cas9-based photoactivatable transcription system. *Chem. Biol*. **22**, 169–174 (2015).
26. Nihongaki, Y., Kawano, F., Nakajima, T. & Sato, M. Photoactivatable CRISPR-Cas9 for optogenetic genome editing. *Nat. Biotechnol*. **33**, 755–760 (2015).
27. Zetsche, B. Volz, S. E. & Zhang, F. A split-Cas9 architecture for inducible genome editing and transcription modulation. *Nat. Biotechnol*. **33**(2), 139–142 (2015).
28. Maji, B. et al. Multidimensional chemical control of CRISPR–Cas9. *Nat. Chem. Biol*. **13**, 9. (2016).
29. Davis, K. M., Pattanayak, V., Thompson, D. B., Zuris, J. A. & Liu, D. R. Small molecule–triggered Cas9 protein with improved genome-editing specificity. *Nat. Chem. Biol*. **11**(5), 316–318. (2015).
30. Hilton, I. B. & Gersbach, C. A. Chemical control for CRISPR editing. *Nat. Chem. Biol*.**13**, 2. (2016).
31. P. K. et al. Development of light-activated CRISPR using guide RNAs with photocleavable protectors. *Angew. Chem. Int. Ed*. **55**, 12440–12444 (2016).
32. Polstein, L. R. & Gersbach, C. A. A light-inducible CRISPR-Cas9 system for control of endogenous gene activation. *Nat. Chem. Biol*. **11**, 198–200 (2015).
33. Bubeck, F. et al. Engineered anti-CRISPR proteins for optogenetic control of CRISPR–Cas9. *Nat. Methods* **15**, 924–927 (2018).
34. Shao, J. et al. Synthetic far-red light-mediated CRISPR-dCas9 device for inducing functional neuronal differentiation. *Proc. Natl. Acad. Sci. USA* **115**, E6722–E6730 (2018).
35. Pan, Y. et al. Near-infrared upconversion–activated CRISPR-Cas9 system: a remote-controlled gene editing platform. *Sci. Adv.* **5**, eaav7199 (2019).
36. Mosser, D. D., Duchaine, J. & Massie, B. The DNA-binding activity of the human heat shock transcription factor is regulated in vivo by hsp70. *Mol. Cell. Biol.* **13**, 5427–5438 (1993).
37. Abravaya, K., Myers, M. P., Murphy, S. P. & Morimoto, R. I. The human heat shock protein hsp70 interacts with HSF, the transcription factor that regulates heat shock gene expression. *Genes Dev.* **6**, 1153–1164 (1992).
38. Li, X. et al. In vitro and in vivo photothermal cancer therapeutic effects of gold nanorods modified with mushroom β-glucan. *J. Agric. Food Chem.* **66**, 4091–4098 (2018).
39. Chen, Y., Zhao, Y., Yoon, S. J., Gambhir, S. S. & Emelianov, S. Miniature gold nanorods for photoacoustic molecular imaging in the second near-infrared optical window. *Nat. Nanotech*. DOI: 10.1038/s41565-019-0392-3 (2019).
40. Hu, Q. et al. Engineering nanoparticle-coated bacteria as oral DNA vaccines for cancer immunotherapy. *Nano Lett.* **15**, 2732–2739 (2015).
41. Wu, M. et al. Targeting ETS1 with RNAi-based supramolecular nanoassemblies for multidrug-resistant breast cancer therapy. *J. Control. Release* **253**, 110–121 (2017).
42. Zhang, Z. et al. Cationic polymer-mediated CRISPR/Cas9 plasmid delivery for genome editing. *Macromol. Rapid Commun.*, 1800068 (2018).
43. Andersson, H. A. et al. HSP70 promoter-driven activation of gene expression for immunotherapy using gold nanorods and near infrared light. *Vaccines* **2**, 216–227 (2014).
44. Vanzetti, L. et al. XPS analysis of genomic DNA adsorbed on PEI-modified surfaces. *Surf. Interface Anal*. **48,** 611-615 (2016).
45. Islam, M. S., Choi, W. S. & Lee, H. J. Controlled etching of internal and external structures of SiO_2 nanoparticles using hydrogen bond of polyelectrolytes. *ACS Appl. Mater. Interfaces* **6**. 12, 9563–9571 (2014).

46. Xiang, G., Zhang, X., An, C., Cheng, C. & Wang, H. Temperature effect on CRISPR-Cas9 mediated genome editing. *J. Genet. Genomics* **44**, 199–205 (2017).
47. Wang, P. et al. Thermo-triggered release of CRISPR-Cas9 system by lipid-encapsulated gold nanoparticles for tumor therapy. *Angew. Chem. Int. Ed.* **57**, 1491–1496 (2018).
48. Ma, W. et al. Dual quantification of microRNAs and telomerase in living cells. *J. Am. Chem. Soc.* **139**, 11752–11759 (2017).
49. Chen, S. et al. Near-infrared deep brain stimulation via upconversion nanoparticle–mediated optogenetics. *Science* **359**, 679–684 (2018).
50. Tan, P., He, L., Han, G. & Zhou, Y. Optogenetic immunomodulation: shedding light on antitumor immunity. *Trends Biotechnol.* **35**, 215–226 (2017).
51. Jiang, Y. et al. Metabolizable semiconducting polymer nanoparticles for second near-infrared photoacoustic imaging. *Adv. Mater.* **31**, 1808166 (2019).
52. Zhu. S., Tian, R., Antaris. A. L., Chen. X. & Dai. H., Near-infrared-II molecular dyes for cancer imaging and surgery. *Adv. Mater.* **14**, 1900321 (2019)
53. Hong, G., Antaris, A. L. & Dai, H.,Near-infrared fluorophores for biomedical imaging. *Nat. Biomed. Eng*. **1**, 0010 (2017).
54. Conde, J., Oliva, N., Zhang, Y. & Artzi, N. Local triple-combination therapy results in tumour regression and prevents recurrence in a colon cancer model. *Nat. Mater.* **15**, 1128–1138 (2016).
55. Hinde, E. et al. Pair correlation microscopy reveals the role of nanoparticle shape in intracellular transport and site of drug release. *Nat. Nanotechnol.* **12**, 81–89 (2017).
56. Morimoto, R. Cells in stress: transcriptional activation of heat shock genes. *Science* **259**, 1409–1410 (1993).
57. Abravaya, K., Phillips, B. & Morimoto, R. I. Attenuation of the heat shock response in HeLa cells is mediated by the release of bound heat shock transcription factor and is modulated by changes in growth and in heat shock temperatures. *Genes Dev.* **5**, 2117–2127 (1991).
58. Lyu, Y. et al. Dendronized semiconducting polymer as photothermal nanocarrier for remote activation of gene expression. *Angew. Chem. Int. Ed*. **56**, 9155–9159 (2017).
59. Miyako, E. et al. Photothermic regulation of gene expression triggered by laser-induced carbon nanohorns. *Proc. Natl Acad. Sci. USA* **109**, 7523–7528 (2012).
60. Nakatsuji, H., Galbraith, K. K., Kurisu, J., Imahori, H., Murakami, T. & Kengaku, M. Surface chemistry for cytosolic gene delivery and photothermal transgene expression by gold nanorods. *Sci. Rep.* **7**, 4694 (2017).
61. Raj, B. et al. Simultaneous single-cell profiling of lineges and cell types in the vertebrate brain. *Nat. Biotechnol.* **36**, 442–450 (2018).
62. Yen, S. T. et al. Somatic mosaicism and allele complexity induced by CRISPR/Cas9 RNA injections in mouse zygotes. *Dev. Biol.* **393**, 3–9 (2014).
63. Wang, H. et al. One-step generation of mice carrying mutations in multiple genes by CRISPR/Cas-mediated genome engineering. *Cell* **153**, 910–918 (2013).
64. Gangopadhyay. S. A. et al. Precision control of CRISPR/Cas9 using small molecules and light. *Biochemistry* **58**, 234–244 (2019).
65. B. Wang, X. Yu, J. Wang, Z. Li, P. Li, H. Wang, L. Song, P. K. Chu, C. Li, Gold-nanorods-siRNA nanoplex for improved photothermal therapy by gene silencing. *Biomaterials* **78**, 27–39 (2016).
66. Li, S. et al. A novel inducible lentiviral system for multi-gene expression with human HSP70 promoter and tetracycline-induced promoter. *Appl. Microbiol. Biotechnol.* **101**, 9, 3689–3702 (2017).

67. Zhou, H. B. et al. In vivo simultaneous transcriptional activation of multiple genes in the brain using CRISPR-dCas9-activator transgenic mice. *Nat. Neurosci.* **21**, 440–446 (2018).

Acknowledgments

The authors gratefully acknowledge the National Natural Science Foundation of China (81872807), Fundamental Research Funds for the Central Universities (2018XZZX001-14), and Thousand Talents Plan (Y.P.), for the financial support of this work. The authors also acknowledge Dr. D. Wu for the helpful discussion on the synthesis of gold nanorod, and S. Zhang for the help in the construction of plasmids.

Author contribution

Y.P. conceived the project and designed experiment. X.C. performed in vitro and in vivo experiments. Y.C. synthesized and characterized polymer-coated gold materials. H.X. constructed the plasmids. T.W., H.X. and Y.P. planned and interpreted the data. Y.P. supervised the project, and wrote manuscript.

Conflict of Interest: The authors declare no conflict of interest.

Additional information

Supplementary material is available for this manuscript.

Fig.s and Schemes

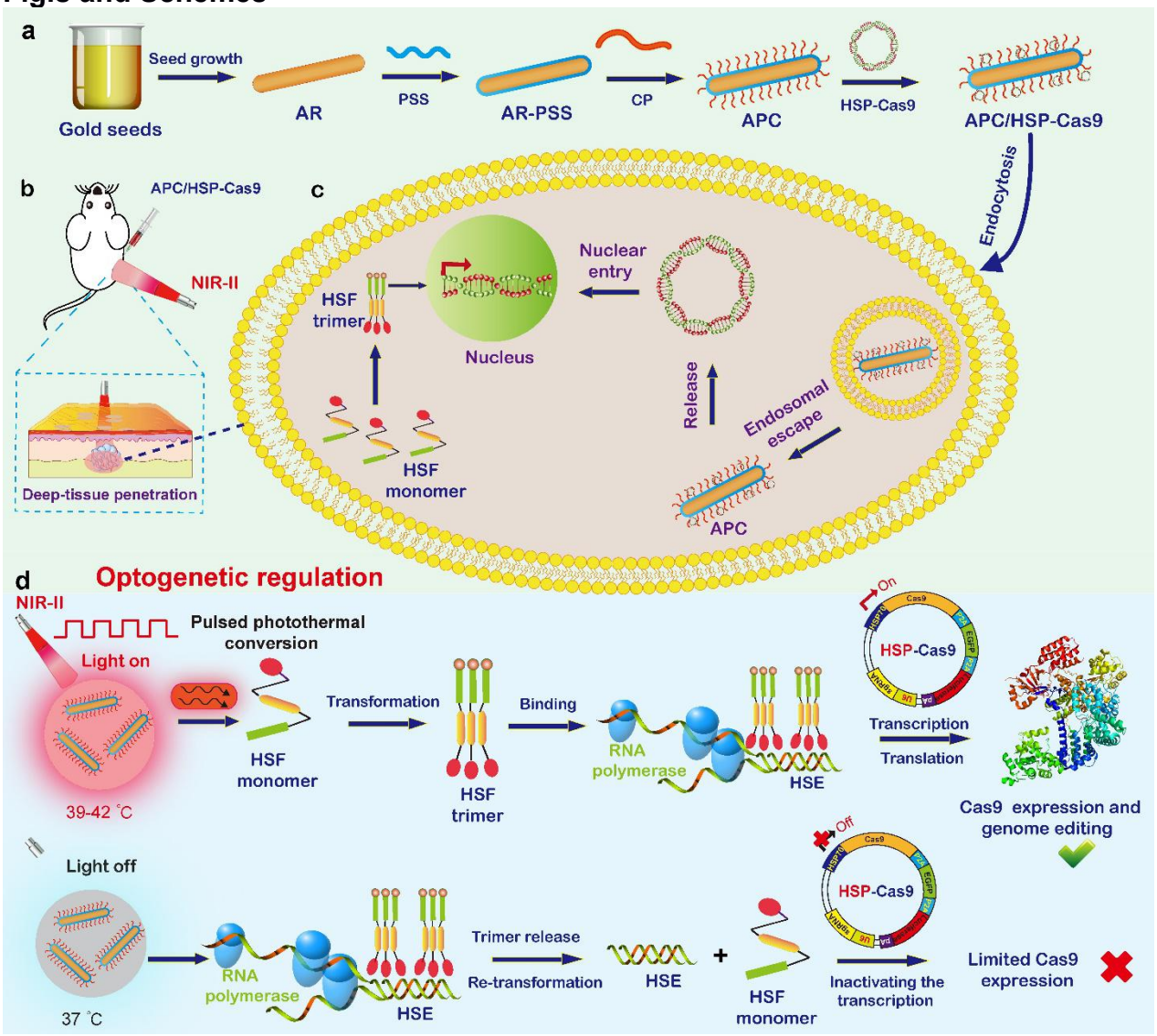

Scheme 1. Illustration of the optogenetic regulation of genome editing mediated by photoactivatable CRISPR/Cas9 nanosystem. **(a)** Process of preparation of APC/HSP complex; **(b)** Illustration of deep-tissue penetration by NIR-II light; **(c)** Intracellular delivery of APC/HSP-Cas9 complexes; **(d)** Mechanism of reversible optogenetic regulation of Cas9 expression and genome editing.

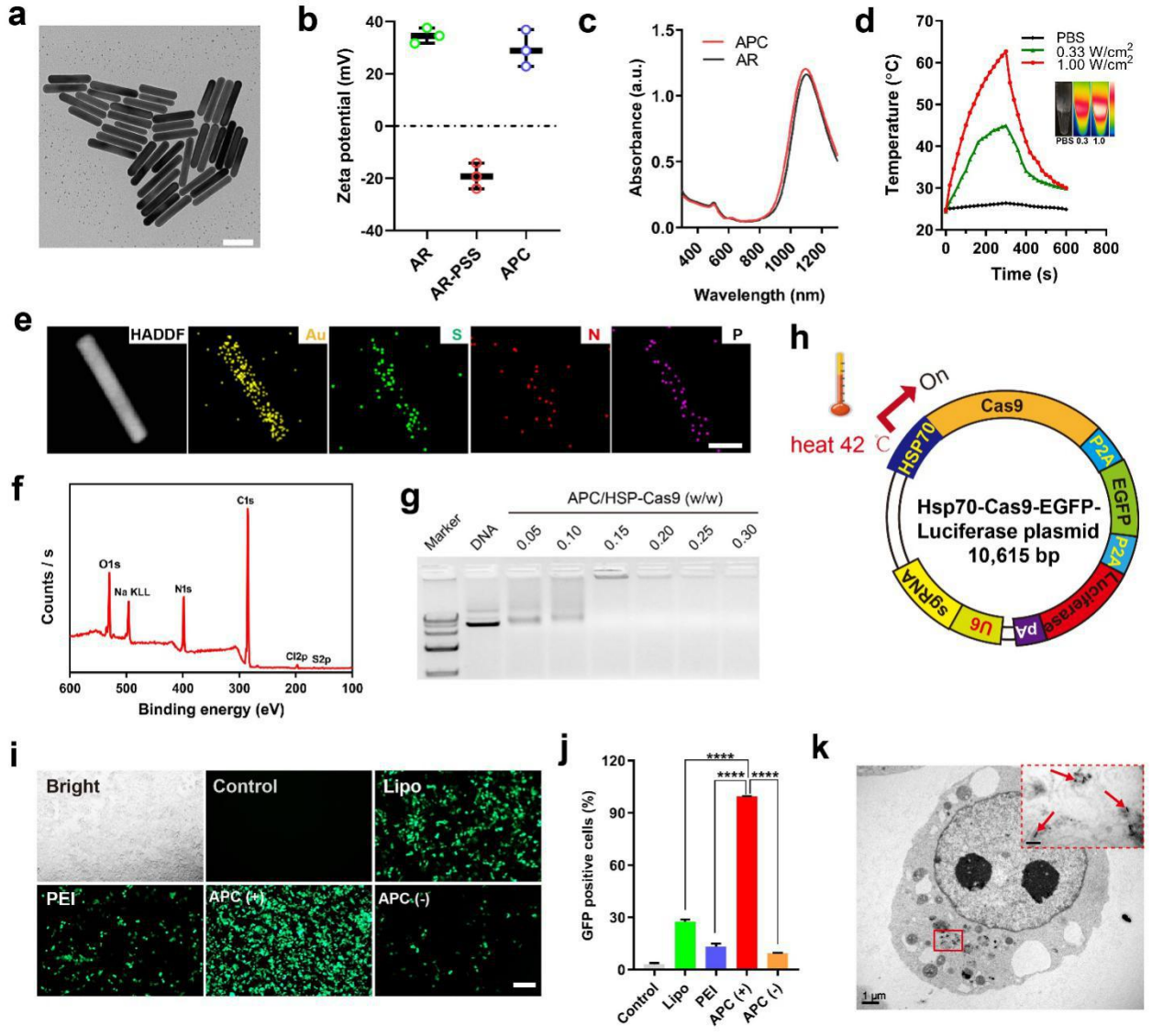

Fig. 1. **Characterization of APC and evaluation of transfection activity**. **a**. TEM image of APC. **b**. Zeta potential analysis of gold nanorods (AR), PSS-coated AR, and APC. Mean ± S.D., n = 3. **c**. Absorption spectrum of AR and APC. **d**. Solution temperature of APC as a function of laser irradiation time. The laser wavelength was 1064 nm. Insert, thermal image of PBS solution at a laser power density of 0.33 W/cm^2 (left), APC solution at a power density of 0.33 W/cm^2 (middle), and 1.00 W/cm^2 (right) at their respective maximum temperature. **e**. HADDF-STEM and EDS mapping of APC/HSP-Cas9. The scale bar indicates 25 nm. **f**. XPS spectra of APC/HSP-Cas9 complexes. **g**. Agarose gel electrophoresis of APC/HSP-Cas9 complexes at various APC/DNA weight ratios. **h.** HSP70 promoter-driven CRISPR/Cas9 plasmid (HSP-Cas9). The plasmid consists of a Cas9 gene driven by a HSP70 promoter, an EGFP reporter and a luciferase reporter downstream of Cas9, separated by self-cleaving peptides P2A. A segment of independent sgRNA sequence which is driven by U6 promoter was further inserted in the downstream of luciferase reporter. **i**. GFP expression mediated by APC/HSP-Cas9 with (+) or without (-) laser irradiation at 1064 nm. Lipo- and PEI-mediated transfections at 42 °C were used as positive controls, whereas cells without any treatment were used as a negative control. The scale bar represents 200 μm. **j**. Flow cytometry analysis of GFP-positive cells. Mean ± S.D., n = 3, *** P < 0.001. **k**. Bio-TEM image of 293T cells after the transfection of APC/HSP-Cas9 complexes. The arrows in the image show the presence of APC in the cytoplasm.

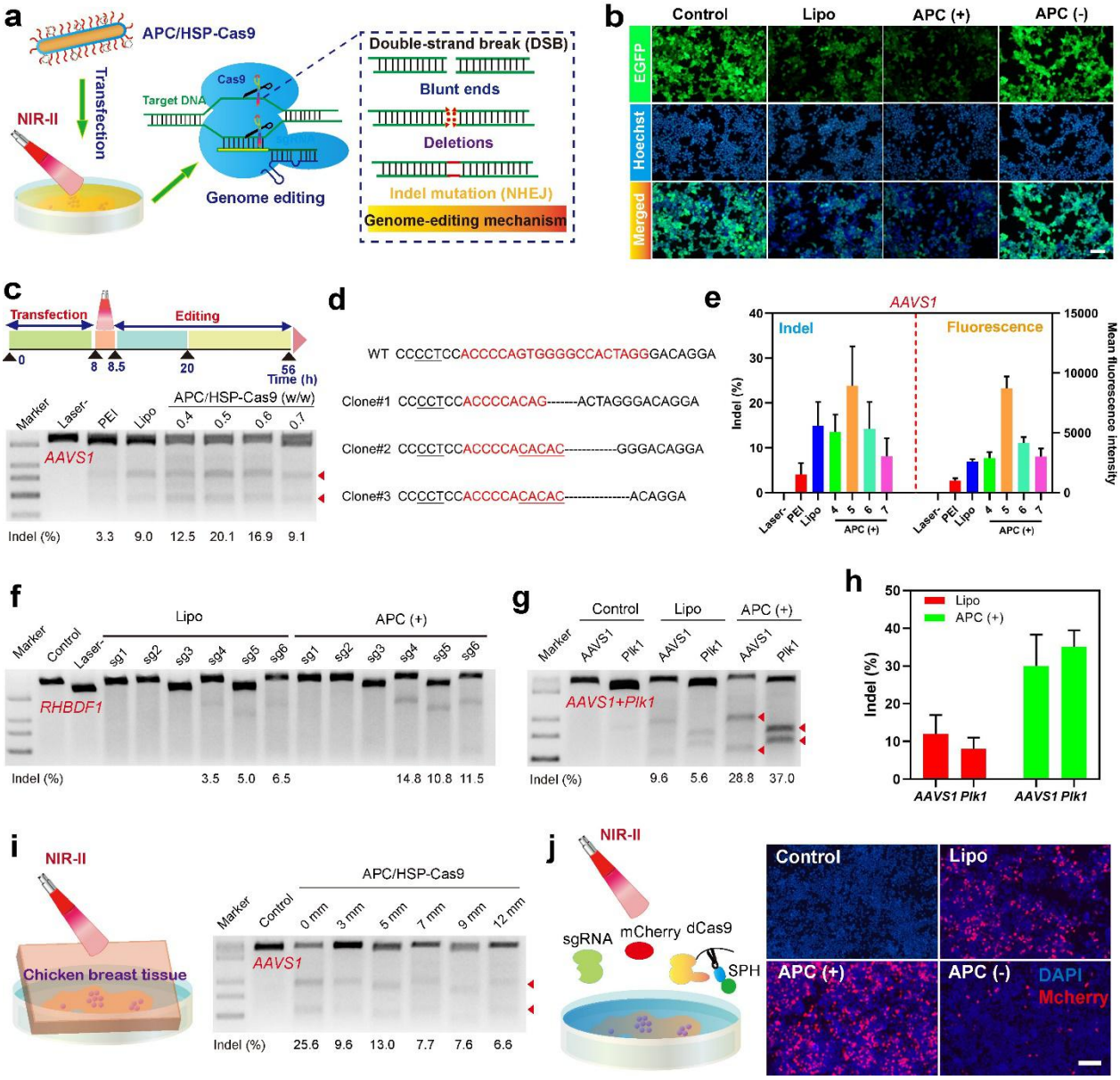

Fig. 2. Optogenetic activation of CRISPR/Cas9 genome editing by APC/HSP-Cas9. a. Illustration of optogenetic activation mediated by APC. **b**. CLSM images of 293T-EGFP cells treated with APC/HSP-Cas9 targeting EGFP, followed by optogenetic activation. Lipo-mediated transfection at 42 °C and APC-mediated transfection without irradiation were used as controls. The scale bar represents 200 μm. **c**. Indel mutations of *AAVS1* locus of 293T cells transfected APC/HSP-Cas9 complexes with or without laser irradiation. APC was complexed with HSP-Cas9 at different weight ratios. Lipo and PEI were used as positive controls. **d.** Sanger sequencing results of T-A cloning from 293T cells (*AAVS1*) after APC-mediated transfection and optogenetic activation. The target sequences were marked in red. PAM was underlined (black). Substitutions, insertions and deletions were marked by red base sequences, underlines (red), and dotted lines, respectively. **e**. Analysis of indel rate, as revealed by the grayscale density of cut bands from T7E1 results, after the transfection of ACP/HSP-Cas9 targeting *AAVS1* with or without laser treatment (left panel). The corresponding GFP expression was evaluated. 4, 5, 6, and 7 refer to APC/HSP-Cas9 weight ratio 0.4, 0.5, 0.6 and 0.7, respectively. Mean ± S.D., n = 3. **f.** Indel mutations from 293T cells transfected APC/HSP-Cas9 targeting *RHBDF1* with or without laser irradiation. **g**. Indel mutation from multiplex genome editing by ASP/HSP-Cas9 targeting *Plk1* and *AAVS1* with the laser irradiation. **h**. Quantitative analysis of indel mutations after the multiplex editing at *Plk1* and *AAVS1* loci after the transfection of APC/HSP-Cas9 and

optogenetic activation in 293T cells. Mean ± S.D., n = 3. **i**. Illustration of cultured cells exposed to the irradiation in the presence of a piece of chicken breast tissue (left). Indel mutations of *AAVS1* locus from 293T transfected with APC/HSP-Cas9, followed by the irradiation in the presence of the breast chicken tissue of different thickness (right). **j**. Illustration of optogenetic regulation of transcriptional activation *in vitro* (left). Optogenetic activation of mCherry expression after the co-transfection of plasmids of HSP-dCas9-SPH, miniCMV-mCherry and U6-sgRNA by APC (right).

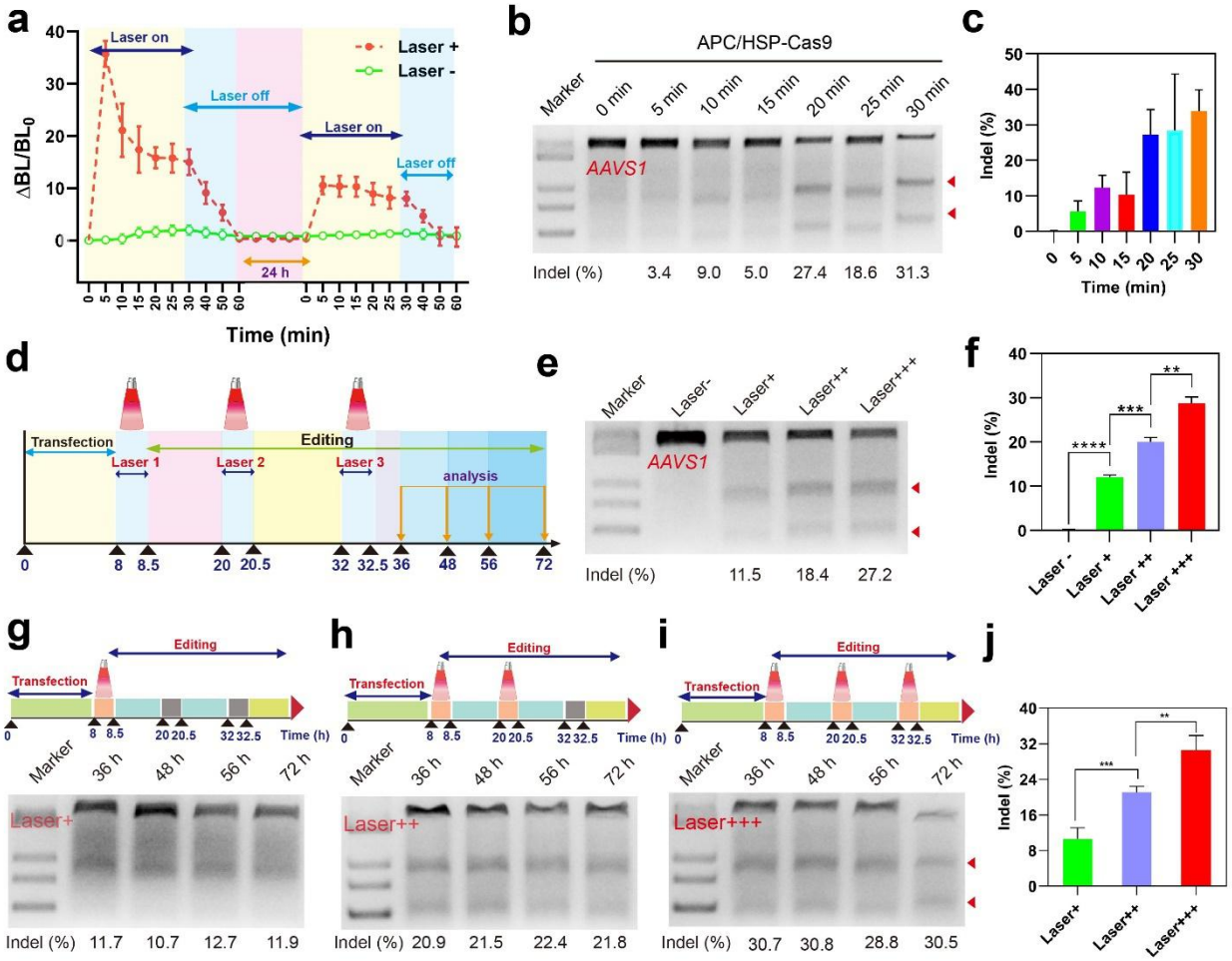

Fig. 3. APC-mediated optogenetic control of programmable genome editing in vitro. a. Quantitative analysis of changes in luminescence intensity. The incremental percentage of BL intensities was monitored as a function of time. **b**. Indel mutations of *AAVS1* locus detected by T7E1 assay. 293T cells were first transfected with APC/HSP-Cas9 complexes, and then exposed to the laser irradiation from 5 to 30 min. The indel mutations were evaluated 72 h after the irradiation. **c**. Quantitative analysis of indel mutations at *AAVS1* locus. The experiment conditions were same as those described in Fig. 3B. Mean ± S.D., n = 3. **d**. Illustration of transfection, irradiation and genome editing processes. The irradiations were conducted at 8 h, 20 h, and 32 h after the transfection, and irradiation time was 30 min each time. The indel analysis was conducted at 36 h, 48 h, 56 h, and 72 h, respectively. **e**. Indel mutations of *AAVS1* locus detected by T7E1 assay. The irradiation was conducted at 8 h (Laser+), 8 h and 20 h (Laser++), and 8 h, 20 h, and 32 h (Laser+++) after the transfection. The indel mutations were analyzed at 72 h after the transfection. **f**. Quantitative analysis of indel mutations at *AAVS1* locus after the transfected cells exposed to the irradiation for different times. Mean ± S.D., n = 3. **g-i**. Indel mutations of *AAVS1* locus detected by T7E1 assay after the exposure to irradiation for different times. The irradiation was conducted at 8 h (Laser+), 8 h and 20 h (Laser++), and 8 h, 20 h, and

32 h (Laser+++) after the transfection, and the cells were harvested at 36 h, 48 h, 56 h, and 72 h for indel analysis. **j**. Quantitative analysis of T7E1 results in Fig. **g-i**. Mean ± S.D., n = 3.

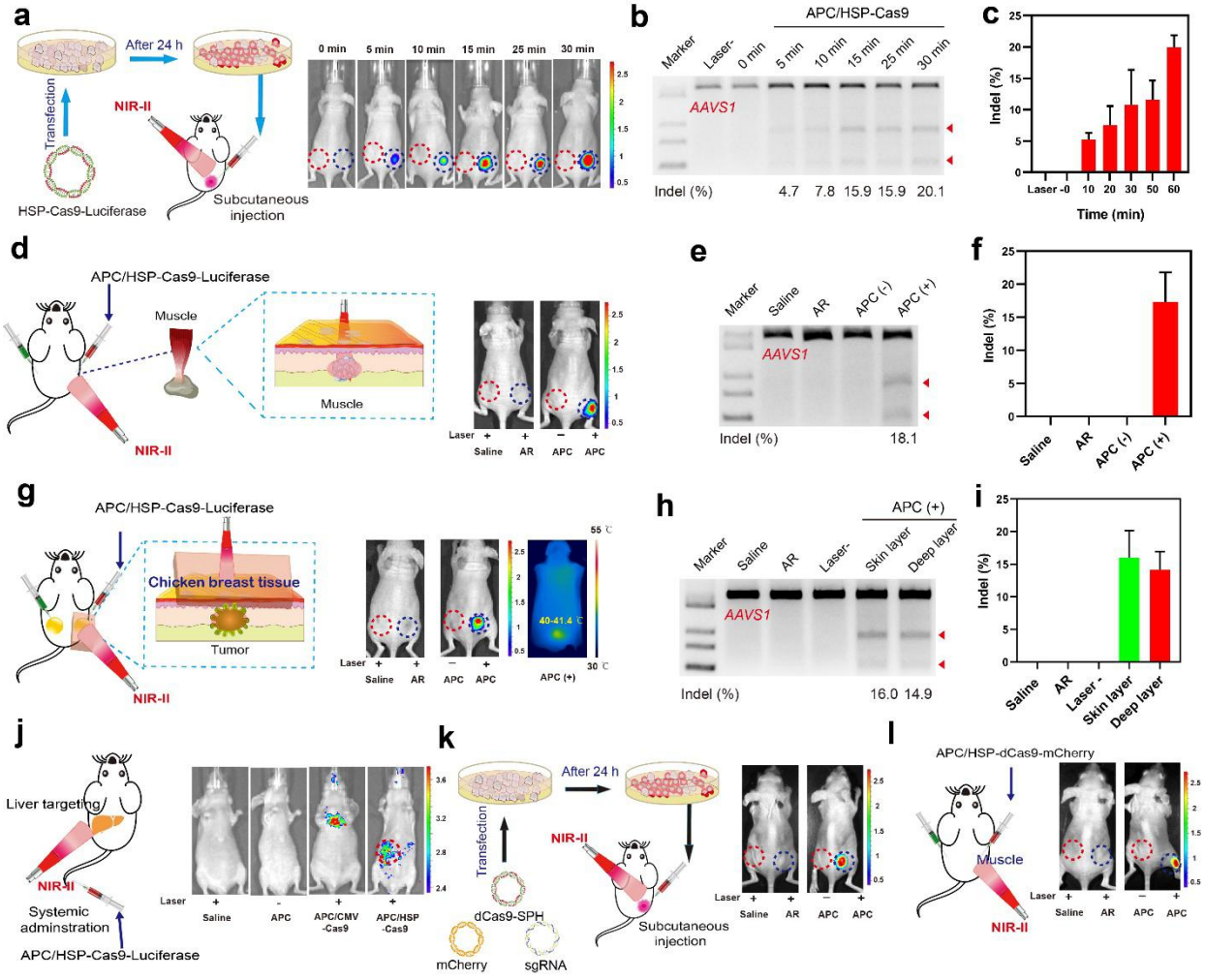

Fig. 4. APC-mediated optogenetic control of programmable genome editing in vivo. (a-c). Evaluation of in vivo genome editing through ex vivo transfection followed by in vivo activation**. a.** Schematic illustration (left). A549 cells were first transfected with APC/HSP-Cas9 complexes, and were then implanted subcutaneously. Whereas the right implanted position was exposed to irradiation from 5 to 30 min, the left position that was not exposed to irradiation was used as the control. In vivo luciferase expression (right). **b**. Indel mutations detected by T7E1 assay. **c**. Quantitative analysis of indel mutations. (**d-f**) Evaluation of direct in vivo transfection followed by optogenetic activation**. d**. Schematic illustration (left). APC/HSP-Cas9 complexes were subcutaneously injected into the muscle of the hind limb of BALB/c mice, followed by the irradiation at 1064 nm. In vivo luciferase expression (right). **e**. Indel mutations detected by T7E1 assay. **f**. Quantitative analysis of indel mutations. (**g-i**) Evaluation of in vivo genome editing through in vivo local transfection followed by optogenetic activation in the tumor tissue**. g.** Schematic illustration (left). Tumor-bearing mice were administered with APC/HSP-Cas9 complexes through peritumoral injection, and the right tumor was then exposed to the irradiation for 30 min. In vivo luciferase expression (middle), and local tumor temperature during the optogenetic process, as monitored by a thermal camera (right). **h**. Indel mutations detected by T7E1 assay. **i**. Quantitative analysis of indel mutations. **j** Evaluation of in vivo luciferase expression through intravenous injection, followed by the optogenetic activation in the liver**.** Schematic illustration (left). BALB/c mice were injected with APC/HSP-Cas9 complexes via tail-vein injection, and the liver position was exposed to the irradiation for 30 min after the

transfection. (**k-l)**. Optogenetic regulation of transcriptional activation. **k**. Schematic illustration. mCherry expression through ex vivo transfection and in vivo optogenetic activation. **l**. mCherry expression through in vivo transfection and optogenetic activation.

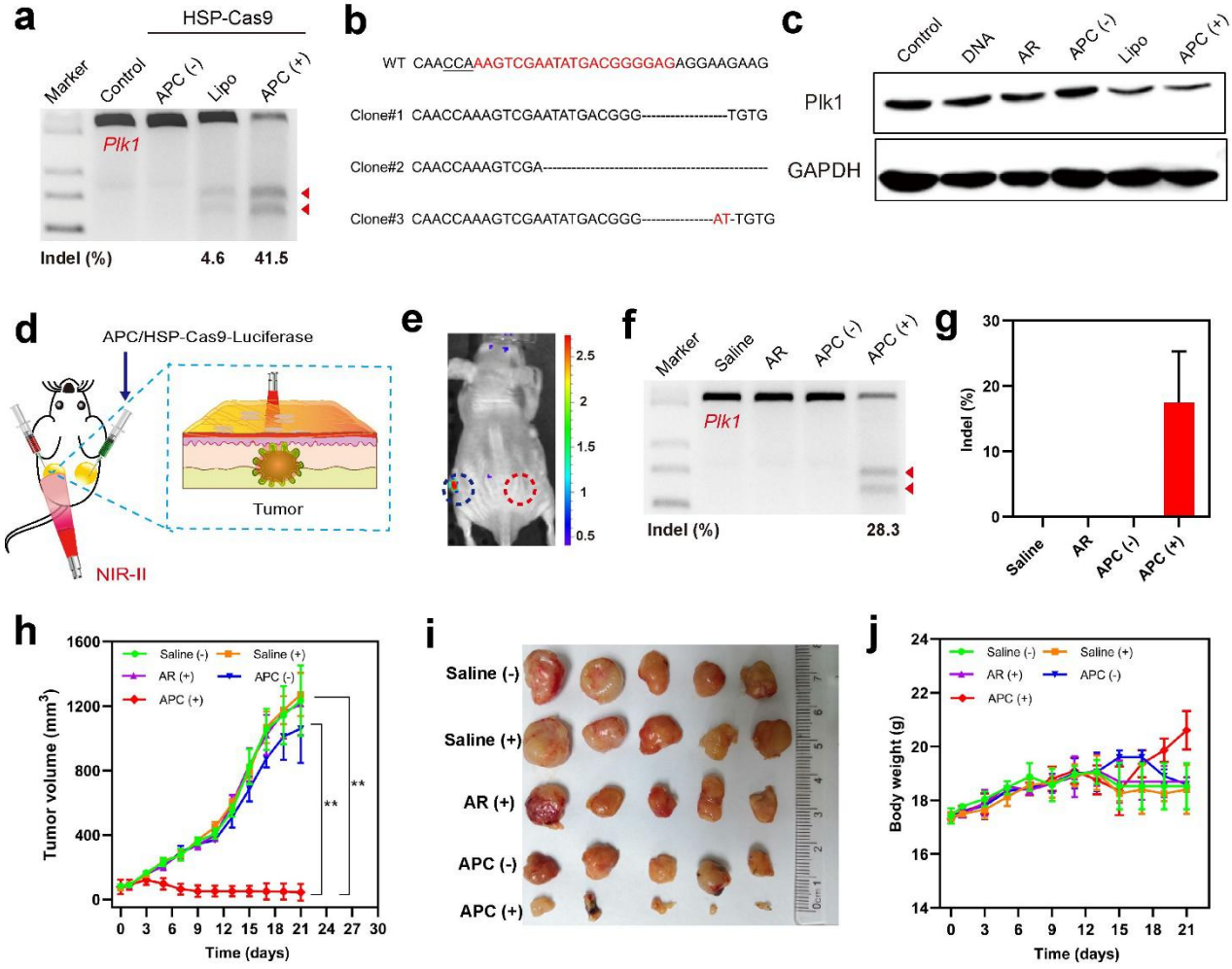

Fig. 5 APC-mediated optogenetic activation for therapeutic genome editing *in vitro* and in vivo. (a-c). In vitro analysis of disruption of *Plk1* gene by optogenetic control of CRISPR/Cas9 genome editing. **a**. Indel mutations detected by T7E1 assay. **b**. Sanger sequencing of T-A cloning results from A549 cell (*Plk1*) by APC-mediated transfection. The target sequences were marked in red. PAM was underlined. Substitutions and deletions were displayed by red base sequences and dotted lines, respectively. **c.** Western blotting analysis of *Plk1* protein expression**. d.** Illustration of optogenetic activation for in vivo cancer therapy. APC/HSP-Cas9 complexes were administered through peritumoral injection, followed by the exposure of tumor to the irradiation. **e**. In vivo luciferase expression in the tumor tissue. The left tumor was exposed to laser irradiation, and the right one without laser exposure was used as the control. **f**. Indel mutations of *Plk1* in the tumor tissue. **g**. Quantitative analysis of indel mutations in the tumor tissue. **h**. The tumor growth curve after the transfection of APC/HSP-Cas9 complexes in the tumor tissue, followed by the exposure to irradiation. The treatment was carried twice a week, and continued for 3 weeks. **i**. The images of dissected tumor tissues from tumor-bearing BALB/c mice with different treatments. **j.** The body weight change during the treatment. Statistical analysis was performed using Students' t-test. All data represent mean ± S.D. (n = 5, **p < 0.01).